79-4056

Numerical Solution of a Body-Propeller Combination Flow Including Swirl and Comparisons with Data

Joseph A. Schetz* and Stanley Favin†
Johns Hopkins University, Laurel, Md.

A numerical procedure based on the full Navier-Stokes equations as applied to the flow near a body/propeller system is developed. The flow is assumed axisymmetric, and the unsteady equations of motion are cast in terms of a stream function, one vorticity component, and the peripheral velocity. The vorticity equation and the peripheral momentum equation are solved by an Alternating Difference Implicit technique, and the Poisson equation for the stream function is solved by direct matrix reduction. The propeller is modeled as an actuator disk, and the direct simulation of a given actual propeller is considered in detail. Turbulent transport is modeled by an integrated Turbulent Kinetic Energy equation with a simple extension to represent the effects of swirl. Detailed comparisons with wind tunnel measurements at $x/D = 2$ show a good prediction of the axial velocity but an underprediction of the swirl level. It is concluded that a more refined turbulence model incorporating a better representation of the effects of swirl is needed. An improved turbulence model can be easily incorporated into the overall calculation procedure when one becomes available.

Nomenclature

a_1, a_2, a_3 = constants in turbulence model
b = mixing zone width
c_2 = constant in turbulence model
F_x = thrust per unit area
F_θ = torque per unit area
H = height of the calculation region
i = index for grid points in the axial direction
j = index for grid points in the radial direction
I_1, I_2, I_3 = integrals in TKE equation
k = turbulent kinetic energy (TKE)
KTH = propeller input parameter
n = index for time step and propeller rpm
Q = total torque
r = radial coordinate
$\bar{r}$ $\equiv r/b$
t = time
T = total thrust
u = axial velocity
$\bar{u}$ $\equiv u/U_e$
$U_e(x)$ = edge velocity
U_∞ = freestream velocity
v = radial velocity
w = peripheral velocity
x = axial coordinate
ξ = vorticity
ψ = stream function
ϵ = eddy viscosity
ρ = density
τ = shear
δ_r^* = displacement thickness
θ = peripheral coordinate
Ω = rotation rate of the propeller
η = propeller efficiency

Subscripts

b, w = on the body

Received March 30, 1978; revision received Sept. 13, 1978.

Index categories: Jets, Wakes and Viscid-Inviscid Flow Interaction; Marine Hydrodynamics

*Consultant; also Professor and Department Head, Aerospace and Ocean Engineering Dept., Virginia Polytechnic Institute and State University.

†Senior Programmer.

Introduction

ANALYSIS of the flowfield produced by a propeller/body combination is of interest in practical applications. Examples include the influence of the propeller on the body pressure distribution to estimate the thrust deduction and the prediction of the near-wake profiles. Until recently, only approximate treatments, e.g., Refs. 1-3, were available. These analyses involved one or more of the following restrictive assumptions: the flow is assumed inviscid; the propeller is represented as an actuator disk with constant thrust; the flow is laminar, and/or the effects of the propeller on the flowfield are small enough to permit a linearization of the equations of motion. The work of Huang (Ref. 4) and Cox (Ref. 5) has attempted to extend these earlier, very approximate analyses.

The numerical solution reported in Ref. 6 had as its goal the development of a realistic treatment, holding simplifying assumptions and approximations to a reasonable minimum. The treatment was based on the full, axisymmetric, mean (in the turbulence sense), unsteady Navier-Stokes equations. In order to place some bounds on the scope of the effort, however, some simplifications were necessary at that time. The first of these was the assumption of an actuator disk model for the propeller, although arbitrary radial variations of thrust were allowed. Also, the propeller could be arbitrarily located in space, so that the effects of rake, etc., could be investigated in detail. Second and perhaps most important, swirl was neglected. Third, turbulent transport processes were described by an integrated, turbulence-kinetic-energy (TKE) equation, which was used to predict an eddy viscosity distribution. The eddy viscosity was allowed to vary only in the streamwise direction.

The purpose of the work reported here was to extend the analysis of Ref. 6 and to undertake detailed comparisons of predictions with available laboratory experimental data. The primary new work was the inclusion of swirling flow as produced by a real propeller. The numerical simulation of a given propeller for the purposes of a calculation like that undertaken here is discussed in detail. Further work on the turbulence transport model was also undertaken.

Analysis

Mathematical Formulation of the Equations of Motion

The mean-flow equations of motion in cylindrical coordinates can be found in standard works such as Ref. 7. For the physical problem of interest here, with the propeller modeled

as an actuator disk, we require the unsteady, axisymmetric (with nonzero peripheral velocity) form of the equations. The work of Ref. 6, which had zero peripheral velocity, was performed using one component of the vorticity (the other two were identically zero) and a stream function as the dependent variables. It has proved convenient, from both a mathematical and numerical sense, to retain the same vorticity-component/stream-function formulation, adding the peripheral velocity as the third dependent variable. With all of this, the equations to be treated may be written as

$$\frac{\partial \xi}{\partial t}+u\frac{\partial \xi}{\partial x}+v\frac{\partial \xi}{\partial r}-\frac{v\xi}{r}+\frac{2w}{r}\frac{\partial w}{\partial x}$$

$$=\epsilon\left(\frac{\partial^2 \xi}{\partial r^2}+\frac{1}{r}\frac{\partial \xi}{\partial r}+\frac{\partial^2 \xi}{\partial x^2}-\frac{\xi}{r^2}\right)+\frac{1}{\rho}\frac{\partial F_x}{\partial r} \tag{1}$$

$$\frac{\partial^2 \psi}{\partial r^2}+\frac{\partial^2 \psi}{\partial x^2}-\frac{1}{r}\frac{\partial \psi}{\partial r}=r\xi \tag{2}$$

$$\frac{\partial w}{\partial t}+u\frac{\partial w}{\partial x}+v\frac{\partial w}{\partial r}+\frac{wv}{r}=\epsilon\left(\frac{\partial^2 w}{\partial r^2}+\frac{1}{r}\frac{\partial w}{\partial r}-\frac{w}{r^2}+\frac{\partial^2 w}{\partial x^2}\right)+\frac{F_\theta}{\rho} \tag{3}$$

The other two velocity components can be determined from

$$ur=\frac{\partial \psi}{\partial r};\quad vr=-\frac{\partial \psi}{\partial x} \tag{4}$$

Here, we have written the equations with a constant turbulent eddy viscosity, ϵ, only for simplicity of presentation. Actually, a variable eddy viscosity was employed in the calculations. The explicit effect of the propeller appears through the axial force term F_x and the peripheral torque term F_θ, which may be arbitrary but differentiable functions of r.

Boundary and Initial Conditions

The boundary conditions used may be written as

$$u(o,r)=u_0(r);\ v(o,r)=v_0(r);\ w(o,r)=0$$

$$\xi(x,H)=w(x,H)=0$$

$$\psi(x,H)=\psi(x,H\text{-}\Delta r)+U_e(x)\cdot(\Delta r)\cdot H$$

$$\frac{\partial^2 \xi}{\partial x^2}(x_f,r)=\frac{\partial^2 \psi}{\partial x^2}(x_f,r)=\frac{\partial^2 w}{\partial w^2}(x_f,r)=0$$

$$w(x,o)=\xi(x,o)=\psi(x,o)=0,\qquad x>x_l$$

$$\psi(x,r_b)=u(x,r_b)=v(x,r_b)=0,\quad 0\le x\le x_l$$

$$w(x,r_b)=0,\quad 0\le x\le x_h,\quad w(x,r_b)=\Omega r,\quad x_h<x\le x_l \tag{5}$$

(See also Fig. 1.)

Note that a spinning propeller hub has been allowed between $x=x_h$ and $x=x_l$.

The boundary conditions on the body cannot be directly restated in terms of the vorticity at the wall; so an iterative procedure is required. Using an expansion procedure, we obtain[6]

$$\xi_w(x)\equiv\left(\frac{\partial u}{\partial r}-\frac{\partial v}{\partial x}\right)_{r=r_b}$$

$$=\frac{2}{r_b}\left(\frac{\psi(x+\Delta x,r_b)}{(\Delta x)^2}+\frac{\psi(x,r_b+\Delta r)}{(\Delta r)^2}\right) \tag{6}$$

At the tail where $r_b=0$, a different expansion is required giving

$$\xi_w(x)=\frac{3\psi(x,\Delta r)}{(\Delta r)^3} \tag{6a}$$

The outer edge boundary conditions as stated in Eqs. (5) are not yet complete, since $U_e(x)$ is involved and unknown. We have adopted the following general procedure to treat the situation (see Ref. 6 for details). First, an exact solution to a related inviscid-flow problem is taken as a base solution. This base solution is then perturbed by an inviscid-viscous interaction to determine the correct velocity distribution, $U_e(x)$, along the outer boundary. An additional benefit arises in that the base inviscid solution can be modified with a boundary layer profile near the body to produce an initial guess with which to begin the whole unsteady calculation.

Simulation of the Propeller

The accurate simulation of a real propeller for the purposes of a calculation like that proposed here is not a trivial exercise. There are important difficulties that must be addressed even after the assumption of an actuator disk model, which eliminates cyclic, unsteady, and detailed three-dimensional effects.

The information required as input for the calculation is $F_x(r)$ and $F_\theta(r)$. While this is an obvious requirement, neither of these quantities is generally known a priori. Indeed, neither the total thrust, the total torque, nor the efficiency of a given propeller operating behind a given body is known unless detailed experiments have been performed. Ordinarily, if such experiments have been performed, there would be no interest in performing subsequent calculations of the type under discussion.

How then, can one proceed? The information that is generally available consists of open-water propeller performance curves and the rpm of the propeller in its operating condition behind the body. The effects of the forebody on the propeller performance can be estimated via the wake fraction method.[8] This itself requires an estimate of the wake profile near the tail of the body. With that procedure, values of the total thrust, torque, and efficiency may be assumed as given (to a somewhat uncertain degree of accuracy). The radial distribution of thrust and torque remains unknown. It has been found useful to employ the well-known rule-of-thumb that the thrust is generally a maximum at 70% of the propeller radius. Also, a simple, blade-element propeller analysis can be used to estimate the appropriate radial distributions. These analyses have proved unreliable for predicting total thrust or torque, but one may hope that the predictions of normalized radial distributions are useful.

If one assumes that the radial distributions of normalized thrust, $F_x(r)/(F_x)_{\max}$, and torque, $F_\theta(r)/(F_\theta)_{\max}$, are the same [$=f(r)$], then the definitions of total thrust and torque

$$T=(F_x)_{\max}r_0^2\int_0^1 2\pi f(r)\left(\frac{r}{r_0}\right)\mathrm{d}\left(\frac{r}{r_0}\right) \tag{7}$$

and

$$Q=(F_\theta)_{\max}r_0^3\int_0^1 2\pi f(r)\left(\frac{r}{r_0}\right)^2\mathrm{d}\left(\frac{r}{r_0}\right) \tag{8}$$

and total efficiency

$$\eta=TU_\infty/2\pi nQ \tag{9}$$

may be combined to give $(F_\theta)_{\max}$ in terms of $(F_x)_{\max}$. Introducing, $KTH\equiv(F_\theta)_{\max}/(F_x)_{\max}$, we obtain

$$KTH=U_\infty/2\pi nr_0\eta \tag{9a}$$

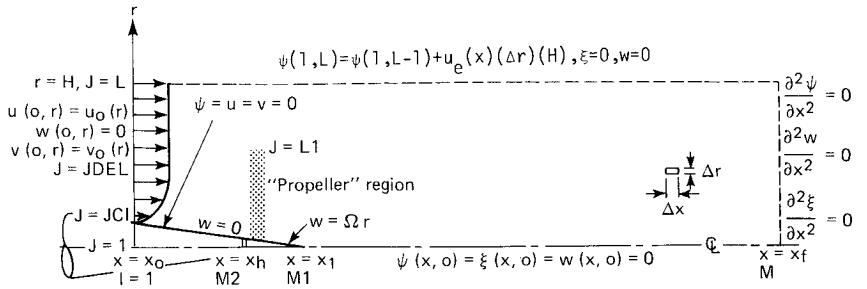

Fig. 1 Schematic of the flowfield and the computational approach.

Turbulent Transport Models

Following the rationale presented in Ref. 6, a simple turbulence model was retained, since there is little experimental turbulence data available for this type of problem on which to base an elaborate model. The approach of McDonald and Camarata[9] as extended by Peters and Phares,[10] where one attempts to calculate the variation of a mean-flow-exchange coefficient (an eddy viscosity or a mixing length) using an integrated form of the turbulence-kinetic-energy equation, has been used. It was not deemed worthwhile to try to accurately resolve the region near the body wall; so an eddy viscosity model that varied with x alone was adopted for most cases.

For the present work, where swirl is to be considered, it was necessary to extend the work of Refs. 6, 9, and 10. Our analysis indicated the need to include the extra term underscored in the equation below.

$$\int_a^{b(x)} \frac{\partial}{\partial x}(\rho u k) r dr = \int_a^{b(x)} -\rho \overline{u'v'} \left(\frac{\partial u}{\partial r}\right) r dr + \int_a^{b(x)} -\rho \overline{w'v'} \left(\frac{\partial w}{\partial r} - \frac{w}{r}\right) r dr - \frac{a_2}{b} \int_a^{b(x)} \rho k^{3/2} r dr \quad (10)$$

where $a=0$ or r_b, the radius of the body.

Adopting a Prandtl eddy viscosity model[11]

$$-\rho \overline{u'v'} = \rho \epsilon \frac{\partial u}{\partial r} = \rho \sqrt{k} l \frac{\partial u}{\partial r} \quad (11)$$

with $l = C_2 b$ and assuming further that

$$-\rho \overline{w'v'} = \rho \epsilon \frac{\partial w}{\partial r} = \rho \sqrt{k} l \frac{\partial w}{\partial r} \quad (12)$$

An ordinary differential equation for $\epsilon(x)$ results:

$$\frac{d\epsilon}{dx} = \frac{C_2^2 U_e}{2}\left(\frac{I_2}{I_1}\right) + \frac{C_2^2 U_e}{2}\left(\frac{I_3}{I_1}\right) - \frac{a_2 \epsilon^2}{4 U_e C_2 b^2 I_1} - \frac{\epsilon}{2 I_1}\frac{dI_1}{dx} + \frac{\epsilon}{2b}\frac{db}{dx} - \frac{\epsilon}{2U_e}\frac{dU_e}{dx} \quad (13)$$

Note that this equation, as written here, is only for the wake where $r_b = 0$ and that

$$I_1(x) \equiv \int_0^l \bar{u} \bar{r} d\bar{r}$$

$$I_2(x) \equiv \int_0^l \left(\frac{\partial \bar{u}}{\partial \bar{r}}\right)^2 \bar{r} d\bar{r}$$

$$I_3(x) \equiv \int_0^l \left[\left(\frac{\partial \bar{w}}{\partial \bar{r}}\right)^2 - \frac{\partial \bar{w}}{\partial \bar{r}}\left(\frac{\bar{w}}{\bar{r}}\right)\right] \bar{r} d\bar{r} \quad (14)$$

The underlined term again indicates the effect of swirl. Typical values of a_2 and C_2 are 1.40 to 2.00 and 0.03 to 0.035.

It is useful here to jump ahead and anticipate some of our actual numerical predictions for the experimental cases of Refs. 12 and 13. The first such calculations were made for the plain, drag-body (propellerless) configuration, which, of course, had no swirl. Comparison of profiles at $x/D=2$ and 5 indicated a somewhat too rapid mixing rate [i.e., too high an $\epsilon(x)$].

Before proceeding, a word of caution is in order. The development of our calculation procedure presupposed the existence of a propeller that would dominate the flow development. Thus, the details of the near-wall region of the body boundary layer were not treated explicitly. If there is no propeller, this near-wall region might be expected to be of first-order importance. A crude attempt at resolving this conflict in philosophy was undertaken. The computer code was modified to include terms introduced by allowing ϵ to vary from a laminar value at the wall to the appropriate $\epsilon(x)$ at the first grid point. This change produced significant effects on the predicted body boundary layer profile but negligible effects on the profiles in the wake at $x/D=2$ and 5. On this, perhaps limited, basis, we concluded that the differences in the predicted profiles and data were indeed due to the basic turbulence model itself and not to the assumption of $\epsilon = f(x)$ alone. One further comment concerning the comparison of prediction and experiment for this case is in order. The calculation assumes a sharp, pointed stern. The experiment was run with the same model as for the propeller-driven model tests; the propeller was simply removed. In either configuration, the downstream end of the body is formed by the propeller hub, which has a blunt tip of about 0.4-in.-diam (the body is 6.0 in. in diameter).

Somewhat more direct evidence to support the contention that the predicted values of $\epsilon(x)$ were too high was found in the turbulence data reported in Ref. 12. The three turbulence intensities were measured and reported, and this information can be used to estimate the average value of the TKE, $\bar{k}$, at $x/D=2$ and 5. Using Eq. (11), we can infer the predicted values of $\sqrt{\bar{k}}$ to be compared with the measured values. This exercise indicated that the predicted values were about 125% high. Equation 11 shows that this can be interpreted as a similar disagreement in $\epsilon(x)$. All of this was with $a_2 = 1.40$ and $C_2 = 0.035$ in the calculations. Other values were also tried. For example, with $a_2 = 2.00$ and $C_2 = 0.035$, the discrepancy between the predicted and inferred values of $\sqrt{\bar{k}}$ was reduced to about 80%. However, the agreement between the predicted and observed velocity profiles was not dramatically improved.

The calculation of $\epsilon(x)$ begins with a value $\epsilon(o)$ derived from the given initial boundary layer on the body and the Clauser[14] outer eddy viscosity model. Observing the predicted downstream development of $\epsilon(x)$ obtained from Eq. (13), we found that the strongest term that produced increases in $\epsilon(x)$ down over the tail and into the wake was the first term on the right-hand side, which itself comes from the first term on the right-hand side of Eq. (10). Peters and Phares[10] and Harsha[15] modeled this type of term differently than via Eq. (11), following Bradshaw et al.[16] Since we had previously had good success with Harsha's code for nonswirling wake cases,[17] consideration was given to modeling the shear term in the TKE equation in the same manner Bradshaw had suggested.

$$-\rho\overline{u'v'} = A_l \rho k \tag{15}$$

for boundary layer flows. Harsha[15] modified the coefficient for jet-wake flows to

$$A_l = a_l \frac{\partial u/\partial r}{|\partial u/\partial r|_{\max}} \quad \text{for} \frac{\partial u}{\partial r} > 0$$

$$A_l = a_l \frac{\partial u/\partial r}{|\partial u/\partial r|_{\min}} \quad \text{for} \frac{\partial u}{\partial r} < 0 \tag{16}$$

The factor a_l is generally taken as 0.3.

Since we wish to consider cases with swirl, it is now necessary to model a second component of the shear. We have simply adopted

$$-\rho\overline{w'v'} = A_\theta \rho k \tag{17}$$

with

$$A_\theta = a_\theta \frac{\partial w/\partial r}{|\partial w/\partial r|_{\max}} \quad \text{for} \frac{\partial w}{\partial r} > 0$$

or

$$A_\theta = a_\theta \frac{\partial w/\partial r}{|\partial w/\partial r|_{\min}} \quad \text{for} \frac{\partial w}{\partial r} < 0 \tag{18}$$

with a_θ expected to be of order 0.3.

At this point, it is important to recognize that we have been led to a hybrid model. Our goal was to predict $\epsilon(x)$ for use in solving the complete Navier-Stokes equations via an integrated TKE equation that involves an average TKE, $\bar{k}(x)$. Here, we have modeled the shear terms in the TKE equation directly through Eqs. (15) and (17). This produces an ordinary differential equation for $\bar{k}(x)$. If we wish to calculate $\epsilon(x)$ from this, we must still use the Prandtl model (or something equivalent):

$$\rho\epsilon(x) = \rho\sqrt{\bar{k}}(x) l = \rho\sqrt{\bar{k}}(x) C_2 b(x) \tag{11a}$$

We have used Eq. (11a). All of this results in a modified form of Eq. (13).

Calculations for the drag-body case mentioned above showed that the disagreement between predicted and measured values of $\sqrt{\bar{k}}$ at $x/D=2$ was reduced to 35% using the modeling in Eqs. (15) and (17). Again, the velocity profiles in the wake were not dramatically improved. We have, however, adopted this modeling of the integrated TKE for future calculations, since the predictions of $\sqrt{\bar{k}}$ are definitely in better agreement with experiment.

Numerical Procedures

The vorticity equation, Eq. (1), is solved for each time step, Δt, in two half-time steps, $\Delta t/2$, using the ADI method of Peaceman and Rachford.[18] The resulting systems of algebraic equations were solved using a library subroutine, LEQT1B, obtained through IMSL. This process involves iteration for the wall vorticity.

The solution to the vorticity equation is then used pointwise for the nonhomogenous right-hand side of the stream function equation, Eq. (2). To solve this equation, the direct reduction method of Buneman[19] as implemented by Swartztrauber and Sweet[20] was employed.

The solution for the peripheral velocity $w(x,r)$ is to be obtained from Eq. (3). Examination of Eqs. (1) and (3) show them to be nearly identical in form, so that the same ADI approach used for Eq. (1) can be applied to Eq. (3). Here, however, there are no iterations, since the value of w on the wall is specified a priori.

The solution procedure can be illustrated by a step-by-step listing showing how the solution is advanced from $t=n(\Delta t)$ to $t=(n+1)(\Delta t)$.

1) Specify F_x, F_θ, and other input quantities. Obtain boundary conditions for ξ^{n+1}, ψ^{n+1}, and w^{n+1}. These are known and usually fixed with time except for ξ_w^{n+1}, which must be iterated for at each time step. The coefficients $u_{i,j}^{n+1/2}$ and $v_{i,j}^{n+1/2}$ in the difference form of Eq. (1) are obtained by extrapolation from the previous time step. The terms involving w are evaluated at time $t=n(\Delta t)$.

2) Solve Eq. (1) using the ADI procedure to obtain ξ^{n+1}.

3) Solve for ψ^{n+1} using the direct solver procedure for Eq. (2) with ξ^{n+1} for the right-hand side.

4) Calculate new values of ξ_w^{n+1} using ψ^{n+1} and Eqs. (6) and (6a).

5) Repeat steps (2)-(4) until ξ_w^{n+1} values converge.

6) Solve for w^{n+1} using the ADI procedure on Eq. (3).

7) Compute u^{n+1} and v^{n+1} from ψ^{n+1} using Eq. (4).

8) Increase or decrease Δt depending on the number of iterations required to determine ξ_w. If fewer than two iterations are required, $(\Delta t)^{n+1} = r(\Delta t)^n$; if more than three iterations are required, $(\Delta t)^{n+1} = (\Delta t)^n / r$.

9) After every five time steps, recalculate $\epsilon(x)$ using Eq. (13), or a modification thereto, and the current velocity profiles. The value of $\epsilon(o)$ at the upstream boundary must be given as a boundary condition. We also recalculate $U_e(x)$ at this time, using the viscid-inviscid interaction procedure developed in Ref. 6.

Results

The laboratory data that are available for comparison with predictions of this calculation procedure are limited. We have selected those in Ref. 13 for use. There were several reasons for this choice; the most important are: 1) the tests were at a reasonably high Reynolds number ($Re_D \approx 4\times10^5$), 2) the body boundary layer profile had been measured ahead of the propeller, 3) propeller performance data (open water) are available, and 4) both mean flow and turbulence profiles were measured in the wake.

First, it is necessary to relate the various input variables and parameters in the calculation procedure to the physical situation. The tests were run in air at $U_\infty = 157$ ft/s and $\rho = 0.07$ lb/ft^3 with a model 72 in. long and 6 in. in diameter. The half-angle of the body tail was 14 deg. The propeller was

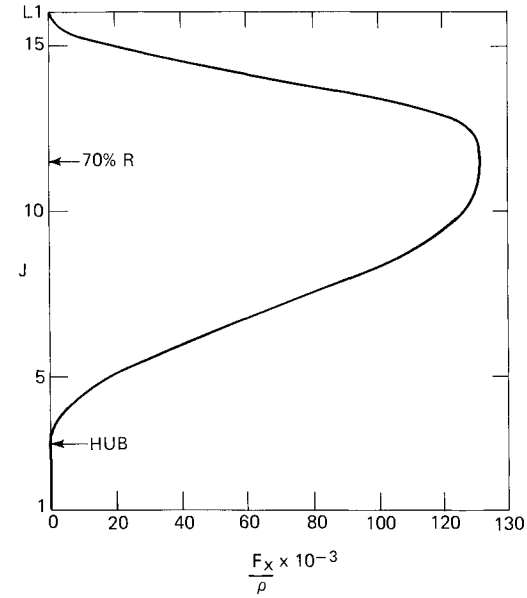

Fig. 2 Radial thrust variation assumed to represent laboratory conditions.

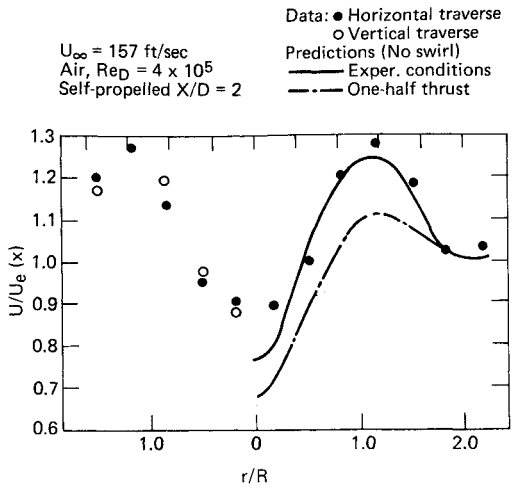

Fig. 3 Comparison of measured and predicted (no swirl) axial velocity profiles at $x/D = 2$.

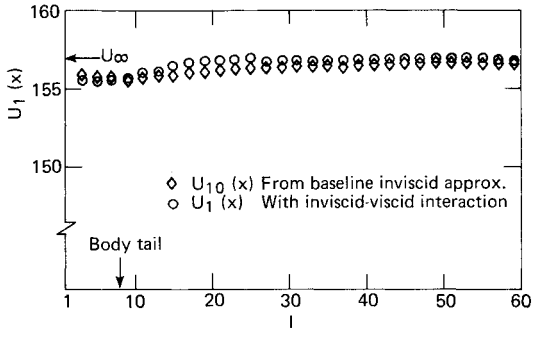

Fig. 4 Velocity variation along the outer boundary of the computation region.

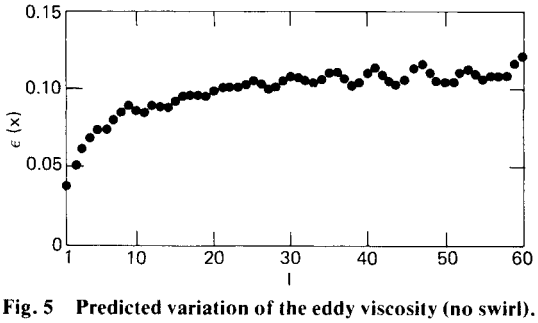

Fig. 5 Predicted variation of the eddy viscosity (no swirl).

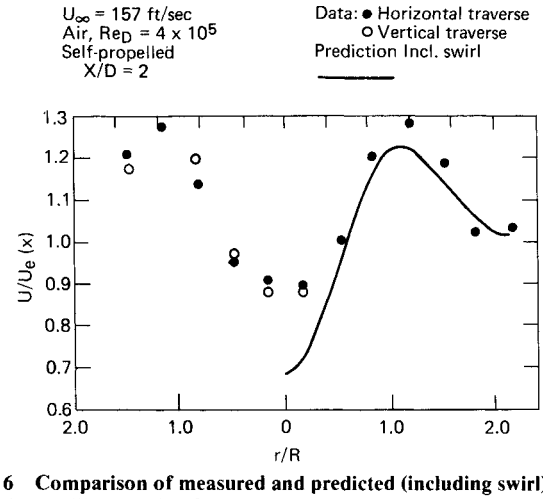

Fig. 6 Comparison of measured and predicted (including swirl) axial velocity profiles at $x/D = 2$.

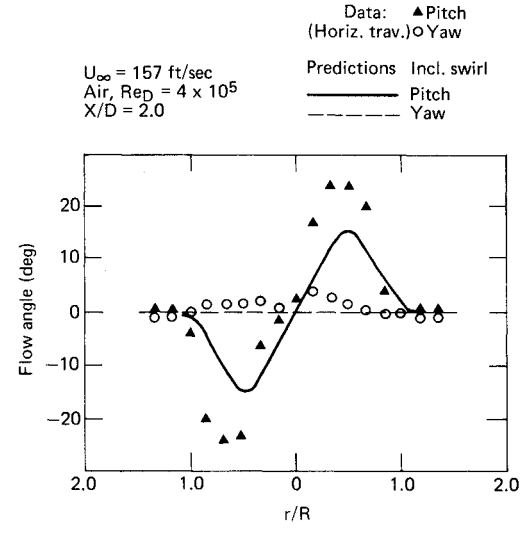

Fig. 7 Comparison of measured and predicted flow angularity at $x/D = 2$.

also 6 in. in diameter. The source/line-sink/uniform-stream solution used in Ref. 6 to develop a baseline inviscid solution to be perturbed along the outer calculation boundary via the viscid-inviscid interaction contains a parameter M related to the strength of the source. The appropriate value for use with a body having the given tail region was determined by trial and error as $M = 27.9 \times 10^{-4}$.

To accurately model the body tail region, propeller diameter, hub length, and initial boundary layer thickness, the following input values were chosen: $\Delta x = 0.0643$ ft, $\Delta r = 0.0167$ ft, and, $L1 = 16$, $M1 = 8$, $M2 = 6$, JCl = 8, JDEL = 13. The outer extent of the calculation region was specified by $L = 30$, $M = 60$. See Fig. 1 for definitions of these quantities.

The specification of the propeller input quantities $F_x(r)$ and $F_\theta(r)$ related to the test conditions is the most indirect part of this whole procedure. The only quantity that we know directly from the tests is propeller rpm = 14,890. The open-water performance curve for this propeller[12] was used to obtain total thrust = 64.4 lb, total torque = 644 in.-lb, and efficiency = 76%. This all resulted in a value of $KTH = 0.785$ via Eq. (9a).

The distribution of thrust over the propeller disk was assumed to peak at approximately 70% of the propeller radius, and the shape of the variation was taken as shown in Fig. 2. This choice of shape is somewhat arbitrary, but it is reasonable. Further, it closely approximates the predictions of a simple blade-element propeller performance code. As noted earlier, the radial variation of peripheral force F_θ was taken as having the same shape as F_x.

The first calculations for the propeller-driven body were made assuming negligible swirl. These results were to serve as a reference case for comparison with the data and the full calculation including swirl. A comparison with the measured velocity profile at $x/D = 2$ is shown in Fig. 3, where quite good agreement except on the axis can be noted. Also shown for reference is the prediction obtained for a total thrust of one-half that actually employed. The inviscid velocity variation along the outer edge of the calculation region is given in Fig. 4, and the predicted variation of $\epsilon(x)$ is given in Fig. 5. The irregularities in the eddy viscosity variation are a result of the calculation of of $b(x)$. The radial station selected as corresponding to $b(x)$ can only occur at a grid point; no interpolation was employed.

Next, calculations attempting a full simulation of the experimental case were run; i.e., swirl velocities were included. The simulation of the influence of the propeller—both thrust and torque—were as described above. The main calculations were run with $a_\theta = 0.30$ by analogy with a_f. The axial velocity distribution obtained at $x/D = 2$ is compared with the data in Fig. 6. Slightly poorer agreement is found in comparison with the prediction obtained neglecting swirl shown in Fig. 3. This is a direct result of the higher eddy viscosity values predicted for the current calculation including swirl.

The prediction of swirl velocity is compared with the data in terms of flow angularity (pitch and yaw) at $x/D = 2$ as shown in Fig. 7. The calculations assume pure axisymmetric flow, so that the prediction for yaw angle for a horizontal traverse is identically zero. The data show some small yaw angle. The prediction for pitch angle is qualitatively correct, but the absolute level of the maximum is too low.

The effect of the value of a_θ was investigated by trying a calculation with $a_\theta = 0.15$. This resulted in lower eddy viscosity values and a slightly improved axial velocity prediction, but somewhat lower pitch angles and therefore slightly poorer agreement with the swirl data.

Discussion

Some aspects of the behavior of the solutions as steady state is approached are worthy of note. The dynamics of the approach to this asymptotic condition are controlled by the iteration on the wall vorticity at each time step. There are two input parameters involved. The first is the tolerance on the maximum percentage change in wall vorticity between iterations before a converged solution at the given time step is judged to have been achieved. It has proved efficient to begin a calculation with a crude tolerance of perhaps 5% and then refine this to 0.5% as steady state is approached. The second parameter is the factor by which the time step is increased or decreased depending on the number of iterations required to obtain a converged wall vorticity. We have used values between 1.05 and 1.30. As steady state is approached, it is necessary to decrease both the tolerance and the time-step factor. If this is not done, the time step will be continuously increased until too large a value is reached, where a converged wall vorticity solution cannot be found in a reasonable number of iterations. The solution does not really diverge either. Typically, it will just miss the tolerance after a few iterations and then proceed along at a level above the tolerance level until stopped by a limit on the maximum number of iterations allowed.

The second aspect of the approach to steady state that is noteworthy was mentioned first in Ref. 6. The propeller seems to produce a mild waviness in the flow which decays slowly with time. We have not observed this phenomenon in flows without a propeller. The present calculations with swirl produced by a propeller also displayed this behavior.

Both of the phenomena mentioned above make difficult a precise judgment as to when steady state has been actually achieved. However, it is not so difficult to judge when a nearly steady-state condition has been obtained where the remaining changes in flow variables with time are quite small.

Our results for swirling cases appear to indicate that there may be required a more elaborate model for turbulent transport including swirl than that obtained here by simple extension of nonswirling models. We have recently learned that other workers (e.g., Ref. 21) have come to a similar conclusion. When a more refined model becomes available, it can be easily incorporated into the present calculation scheme.

Acknowledgment

This work was supported by U.S. Navy Contract N00017-72-C-4401.

References

[1] Von Karman, T. and Burgers, J.M., "General Aerodynamic Theory—Perfect Fluids," *Aerodynamic Theory,* Vol. 2, edited by W.F. Durand, California Institute of Technology, (1934), pp. 104-112.

[2] Sparenberg, J.A., "On the Potential Theory of the Interaction of an Actuator Disk and a Body," *Journal of Ship Research,* Dec. 1972.

[3] Sparenberg, J.A., "On the Linear Theory of an Actuator Disk in a Viscous Fluid," *Journal of Ship Research,* March 1974.

[4] Huang, T. et al., "Propeller/Stern/Boundary-Layer Interaction on axisymmetric Bodies," DTNSRDC Rept. 76-0113, Dec. 1976.

[5] Cox, B.D. and Hansen, A.G., "A Method for Predicting Thrust Deduction Using Propeller Lifting Surface Theory," DTNSRDC Rept. 77-0087, Nov. 1977.

[6] Schetz, J.A. and Favin, S., "Numerical Solution for the Near Wake of a Body with Propeller," *Journal of Hydronautics,* Vol. 11, No. 4, Oct. 1977, pp. 136-141.

[7] Bird, R.B., Stewart, W.E., and Lightfoot, E.N., *Transport Phenomena,* Wiley, New York, 1960, Chap. 3.

[8] Saunders, H.E., *Hydrodynamics in Ship Design,* SNAME, New York, 1957.

[9] McDonald, H. and Camarata, F.J., "An Extended Mixing Length Approach for Computing Turbulent Boundary Layer Development," *AFOSR-IFP Stanford Conference on Turbulent Boundary Layer Prediction,* Stanford, Calif., 1968.

[10] Peters, C. and Phares, W.J., "An Integral Turbulent Kinetic Energy Analysis of Free Shear Flows," *Proceedings of the 1972 NASA-Langley Working Conference on Free Turbulent Mixing,* NASA SP-321, 1972.

[11] Prandtl, L., "Uber ein neues Formelsystem der ausgebildeten Turbulenz," *Nach. Akad. Wiss. Gottingen,* Vol. 6, 1945.

[12] Schetz, J.A. and Jakubowski, A.K., "Experimental Studies of the Turbulent Wake Behind Self-Propelled Slender Bodies," *AIAA Journal,* Dec. 1975, pp. 1568-1575.

[13] Schetz, J.A., Daffan, E.B., and Jakubowski, A.K., "The Turbulent Wake behind Slender Propeller-Driven Bodies at Angle of Attack," AIAA Paper 77-133, Jan. 1977.

[14] Clauser, F.H., "The Turbulent Boundary Layer," *Advances in Applied Mechanics,* Vol. 4, Academic Press, New York, 1956.

[15] Harsha, P.T., "Prediction of Free Turbulent Mixing Using a Turbulent Kinetic Energy Method," *Proceedings of the 1972 NASA-Langley Working Conference on Free Turbulent Mixing,* NASA SP-321, 1972.

[16] Bradshaw, P., Ferriss, D.H., and Atwell, N.P., "Calculation of Boundary Layer Development Using the Turbulent Energy Equation," *Journal of Fluid Mechanics,* Vol. 28, 1967, pp. 593-616.

[17] Swanson, R.C., Jr., and Schetz, J.A., "Calculations of the Turbulent Wake behind Slender Self-Propelled Bodies with a Kinetic Energy Method," *Journal of Hydronautics,* Vol. 9, No. 2, April 1975, pp. 78-80.

[18] Peaceman, D.W., and Rachford, H.H., "The Numerical Solution of Parabolic and Elliptic Differential Equations," *J. Soc. and Appl. Math.,* Vol. 3, 1955.

[19] Buzbee, B., et al., "The Direct Solution of the Discrete Poisson Equation on Irregular Regions," *Siam J. Num. Anal.,* Vol. 8, 1971.

[20] Swartztrauber, P. and Sweet, R., "Efficient FORTRAN Subprograms for the Solution of Elliptic Partial Differential Equations," NCAR TN/IA-109, 1975.

[21] Rodi, W., private communication.